High-resolution isotope-shift spectroscopy of Cd I

Simon Hofsäss [ORCID],[1,*] J. Eduardo Padilla-Castillo [ORCID],[1] Sid C. Wright [ORCID],[1] Sebastian Kray [ORCID],[1] Russell Thomas [ORCID],[1]
Boris G. Sartakov [ORCID],[1] Ben Ohayon [ORCID],[2] Gerard Meijer [ORCID],[1] and Stefan Truppe [ORCID][1,†]

[1]*Fritz-Haber-Institut der Max-Planck-Gesellschaft, Faradayweg 4-6, 14195 Berlin, Germany*
[2]*Institute for Particle Physics and Astrophysics, ETH Zürich, 8093 Zürich, Switzerland*

We present absolute frequency measurements of the $^1P_1 \leftarrow {}^1S_0$ (229-nm) and $^3P_1 \leftarrow {}^1S_0$ (326-nm) transitions for all naturally occurring isotopes of cadmium. The isotope shifts and hyperfine intervals of the fermionic isotopes are determined with an accuracy of 3.3 MHz. We find that quantum interference in the laser-induced fluorescence spectra of the $^1P_1 \leftarrow {}^1S_0$ transition causes a variation of up to 29(5) MHz in determining the hyperfine splitting when not accounted for with an appropriate model. Using a King-plot analysis, we extract the field- and mass-shift parameters and determine nuclear charge radius differences for the fermions. The lifetime of the $^1P_1$ state is determined to be 1.60(5) ns by measuring the natural linewidth of the $^1P_1 \leftarrow {}^1S_0$ transition. These results resolve significant discrepancies among previous measurements.

I. INTRODUCTION

The energy differences between isotopes of an atom or molecule are called isotope shifts (ISs). In atoms, the change in energy has two main contributions: the mass shift (MS) and the field shift (FS). The mass shift is caused by changes in the electronic wave function upon altering the nuclear mass, whereas the field shift arises from changes in the nuclear charge distribution [1]. The shifts in the energy levels can be probed spectroscopically and if the ISs are caused by the MS and FS only, there is a linear relationship between the ISs of two transitions, known as the King plot linearity. Small deviations from this linearity can be a sensitive probe for higher-order terms in the mass shift, the quadratic field shift or isotope-dependent nuclear deformation. In addition, precise values for the MS and FS factors, and deviations from the expected linear behavior of the King plot, provide a useful benchmark for atomic structure calculations.

Recently, it has been suggested that nonlinearities in a King plot can arise from physics beyond the standard model (BSM) of particle physics [2–4]. A new intra-atomic force between a neutron and an electron, mediated by a new boson, can lead to an isotope-dependent energy shift and the introduction of a Yukawa-type particle shift results in a nonlinear King plot [5]. However, this method of searching for new physics relies on a detailed knowledge of the standard model contributions. The Cd atom has recently attracted attention as a sensitive probe

for new physics because of its six even-even isotopes (even number of protons and neutrons) that have a high natural abundance [6]. In addition, the Cd nucleus ($Z = 48$) is only one proton pair below the $Z = 50$ proton shell closure. This significantly reduces potential nonlinearities that arise from a deformed nucleus, which currently limits the interpretation of isotope-shift measurements with Yb [7,8]. Cd possesses a strong cooling transition and weak intercombination lines that can be used for narrow-line cooling, precision spectroscopy, and metrology [9,10], ideal for a sensitive search for BSM physics.

We recently showed that combining precise isotope-shift spectroscopy with new state-of-the-art atomic structure calculations, allows determining the differences in the radii of the nuclear charge distribution with high accuracy [6]. This provides an alternative, independent method to muonic x-ray spectroscopy or electron scattering. The charge radius is a fundamental property of the atomic nucleus, and precise measurements of small differences between isotopes through optical spectroscopy provide stringent tests for nuclear theory [11,12]. In addition, highly accurate charge radii differences are critical to understanding the nuclear contributions to nonlinearities in a King plot.

Here, we present the spectroscopic method used in Ref. [6] to determine ISs of the bosonic $^1P_1 \leftarrow {}^1S_0$ and $^3P_1 \leftarrow {}^1S_0$ transitions in Cd I and combine our previous results with new measurements of the fermionic isotopes ^{111}Cd and ^{113}Cd. For the $^1P_1 \leftarrow {}^1S_0$ transition, we use enriched Cd ablation targets and polarization-dependent spectroscopy to assign spectral lines of different isotopes that otherwise overlap. We measure the hyperfine intervals in the $^1P_1$ state of the two stable fermionic isotopes ^{111,113}Cd with megahertz accuracy by analyzing subtle quantum interference effects in the laser-induced fluorescence (LIF). Knowledge of the exact line shape allows us to significantly improve the ISs and resolve significant discrepancies among previous measurements. The radiative lifetime of the $^1P_1$ state is extracted by fitting the spectral

---

*Corresponding author: hofsaess@fhi-berlin.mpg.de

†Present address: Centre for Cold Matter, Blackett Laboratory, Imperial College London, London SW7 2AZ, United Kingdom.

line shape. The absolute transition frequencies are determined with high accuracy. A King-plot analysis of the two transitions allows extracting the intercept and slope and to determine precise values for the differences in the nuclear charge radii of the fermions. This measurement is also used to benchmark recent state-of-the-art atomic structure calculation of the MS and FS with which we find excellent agreement [13]. In addition, we show that the off-diagonal second-order hyperfine interaction in the fermions is $\lesssim 3$ MHz, in good agreement with calculations [13].

The methods presented here are relevant to the field of collinear laser spectroscopy of rare isotopes produced at accelerator facilities [14]. In these experiments, laser spectroscopy is used to determine the fundamental properties of nuclei, including the nuclear spin, the magnetic dipole moment, the electric quadrupole moment, and the charge radius. Due to the low number of atoms produced in such experiments, these properties are often obtained from strong transitions in the visible or UV part of the spectrum to increase the signal-to-noise ratio. We show that quantum interference in the laser-induced fluorescence of strong transitions can cause significant systematic errors in determining the fundamental properties of nuclei.

II. EXPERIMENTAL SETUP

Figure 1(a) shows a schematic of the experimental setup. We use a cryogenic buffer gas beam source to produce a slow, pulsed beam of Cd atoms with a brightness of about 10^{13} atoms per steradian per pulse and a forward velocity of 100–150 m/s [15,16]. A 1064-nm beam from a pulsed Nd:YAG laser (1 Hz, ≈ 20 mJ in 5–7 ns, ≈ 0.7-mm spot diameter) is focused onto a solid Cd metal target and creates a hot cloud of atoms by laser ablation. We use a multisample target holder, enabling fast switching between targets with different isotopic compositions. The vaporized atoms are cooled by a continuous flow of 1 standard cubic centimeter per minute (1 sccm) cryogenic helium buffer gas (3 K) and are extracted into a beam through a 4-mm aperture in the buffer gas cell. Charcoal-coated copper shields act as a sorption pump for the buffer gas to keep the pressure in the low 10^{-7}-mbar range. The atomic beam is probed in a LIF detector located 0.73 m from the source aperture. A slit with a width of 2 mm along x restricts the transverse velocities of the atomic beam entering the LIF detector. This reduces the Doppler broadening of the $^1P_1 \leftarrow {}^1S_0$ transition to below 2.7 MHz for a forward velocity of 150 m/s. To excite the $^1P_1 \leftarrow {}^1S_0$ transition, we use a frequency-quadrupled continuous-wave titanium-sapphire (Ti:Sa) laser that can generate up to 200 mW at 229 nm. For the $^3P_1 \leftarrow {}^1S_0$ transition at 326 nm, we use a frequency-doubled continuous-wave ring-dye laser (Sirah Matisse 2DX) with a frequency-doubling module (Spectra Physics; Wavetrain) and a Pound-Drever-Hall locking scheme. This laser is stabilized to a linewidth of 100 kHz using a temperature-stabilized reference cavity. The maximum output power is 80 mW in the UV. The laser polarization is purified with an α-BBO ($1:10^5$ extinction ratio). The angle of the linear laser polarization with respect to the detector axis θ_D can be adjusted with a $\lambda/2$ wave plate. LIF of atoms that pass through the detection zone is detected with a photomultiplier-tube
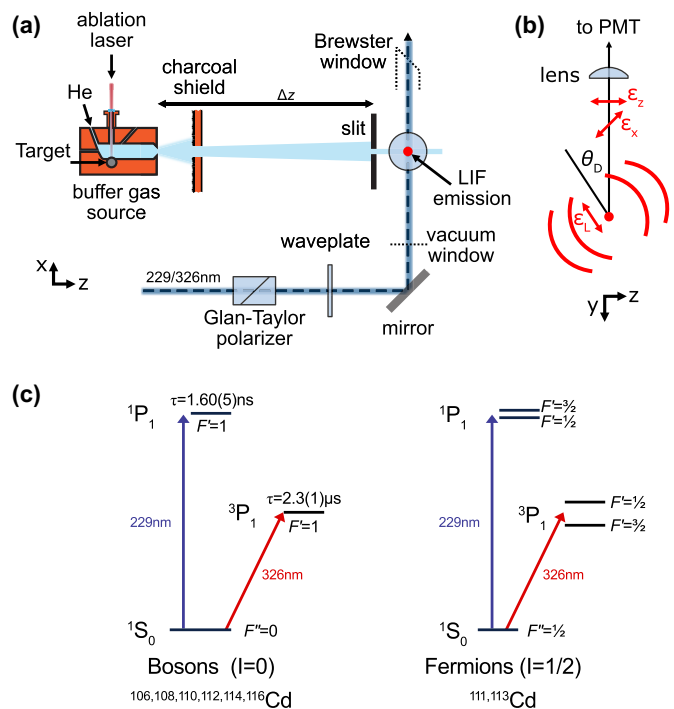

FIG. 1. (a) A collimated atomic beam from a pulsed cryogenic buffer gas source crosses the beam of a continuous wave UV laser at $\Delta z = 0.73$ m. The laser polarization is cleaned up with a Glan-Taylor polarizer and is varied using a wave plate. (b) LIF is detected with a PMT. The linear laser polarization (ϵ_L) forms an angle θ_D with the detector axis. Emitted photons are polarized along $\epsilon_{x,z}$. (c) Energy-level diagram for naturally abundant cadmium isotopes.

(PMT). The laser beam exits the chamber through a Brewster window to avoid backreflection into the interaction zone.

For the $^1P_1 \leftarrow {}^1S_0$ transition, we use a laser beam with a diameter of 5 mm, nearly uniform intensity distribution, and a laser power of 0.5 mW. This corresponds to a saturation parameter of $s_0 = I_{\text{peak}}/I_{\text{sat}} \approx 1/400$, where $I_{\text{sat}} = \pi hc\Gamma/(3\lambda^3) = 1.1$ W cm^{-2} is the two-level saturation intensity and $\Gamma = 1/\tau$ with $\tau = 1.60(5)$ ns being the excited-state lifetime (see below). The scattering rate for small s_0 on resonance is approximately $s_0\Gamma/2 \approx 0.79$ $(\mu s)^{-1}$. The mean interaction time of the atoms with the laser beam is about 30 μs so that each atom scatters on average 24 photons. This results in a radiation-pressure-induced Doppler shift of 1.7 MHz. In relative measurements, such a shift is smaller than our statistical error; for absolute measurements, it is negligible compared to the absolute uncertainty of the wavemeter. For the $^3P_1 \leftarrow {}^1S_0$ transition, 1 mW of laser power in a Gaussian beam with a spot size of 10 mm ($s_0 \approx 10$) is sufficient to saturate the transition. The Doppler broadening due to the transverse velocity distribution in the detector is 1.5 MHz and the radiation pressure detuning due to the scattering of 10 photons is 0.33 MHz.

The laser wavelengths are measured with a wave meter (HighFinesse WS8-10) that is referenced to a calibrated frequency-stabilized HeNe laser at 633 nm and has a resolution of 0.4 MHz. For the 229-nm transition, we measure the frequency-doubled wavelength near 458 nm, whereas
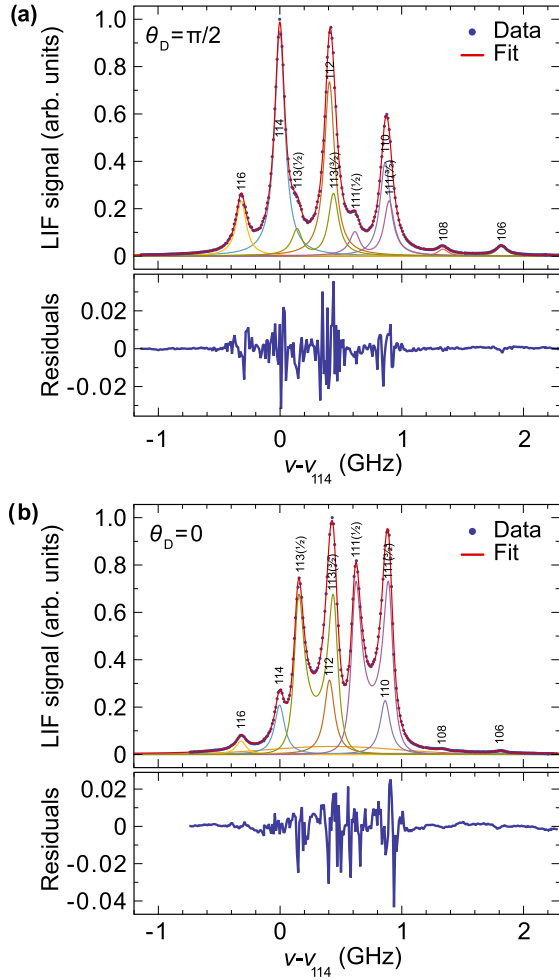
FIG. 2. Isotope-shift spectrum of the $^1P_1 \leftarrow {}^1S_0$ transition at 229 nm relative to ^{114}Cd, measured under two different laser polarizations angles, fitted with the quantum interference model for fermions. The fit residuals are shown below the respective plot. (a) $\theta_D = \pi/2$ maximizes the laser-induced fluorescence emission of the bosons towards the detector. (b) $\theta_D = 0$ suppresses the fluorescence emission of the bosons and, thus, improves the accuracy in determining the transition frequencies of the fermions.

for the 326 nm we measure the fundamental wavelength near 652 nm.

III. ATOMIC BEAM SPECTROSCOPY

This section is split into three parts. In Sec. III A we show measured spectra of the $^1P_1 \leftarrow {}^1S_0$ and $^3P_1 \leftarrow {}^1S_0$ transitions and explain the experimental and data analysis methods used. We benchmark a sophisticated model for the line shape of the fermions and measure the linewidth of the $^1P_1 \leftarrow {}^1S_0$ transition to infer the lifetime of the $^1P_1$ state. Section III B focuses on systematic uncertainty, which is the limiting factor in the accuracy of our measurements. We compare our measurements in Cd with known properties of the hyperfine intervals of the $^3P_1$ state and measure well-known transitions in atomic copper at nearby wavelengths. Finally, the accuracy of relative measurements is established by probing the linearity of our wave meter with an ultrastable cavity. In Sec. III C we discuss
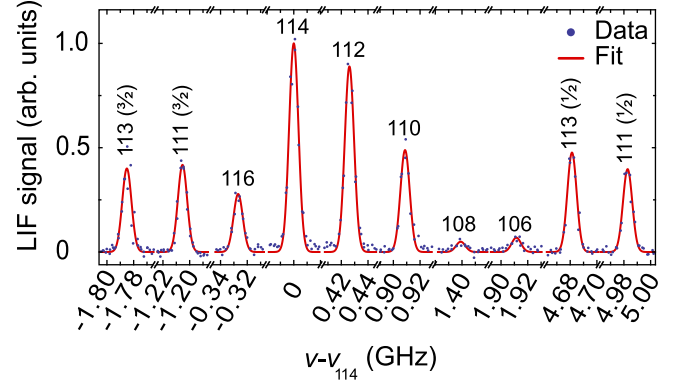

FIG. 3. Representative spectrum for 326 nm relative to ^{114}Cd. The excited-state hyperfine level of fermionic isotopes is indicated in brackets.

the results, analyze them in a King plot and calculate the nuclear charge radius differences for the fermions.

A. Measurements

Figure 2 shows two fluorescence spectra around 229 nm for two different laser polarization angles θ_D. The natural linewidth of the $^1P_1 \leftarrow {}^1S_0$ transition and the hyperfine splitting of the fermionic isotopes (Δ_{HF}) in Cd are of the same order of magnitude as the ISs. The result is a spectrum with a significant overlap of the spectral lines. This overlap complicates the determination of the resonance frequencies, making them dependent on the precise determination of the line shape. The methods we use to mitigate these complications are presented in Sec. III A 1.

A typical spectrum for the 326-nm line is shown in Fig. 3. The line shape is dominated by Gaussian broadening with a full width at half maximum of 4.1 MHz. There is no spectral overlap between the lines and the excited-state hyperfine levels of the fermionic isotopes are split by approximately $10^5\Gamma$ with negligible influence of quantum interference. When the laser beam is not orthogonal to the atomic beam, the spectrum of atoms with a high forward velocity is shifted with respect to atoms with a low forward velocity. By changing the alignment of the laser beam to overlap the spectra, we reduce the residual Doppler shift to $\leqslant 1$ MHz. We fit a Gaussian function to the spectral lines and determine the line centers with a statistical uncertainty of better than 1 MHz. The results are summarized in Table I.

1. Spectral line shape

All stable bosonic isotopes of cadmium have nuclear spin $I = 0$, and their fluorescence emission pattern corresponds to that of a classical Hertzian dipole. When the atoms are excited with linearly polarized light and the detection direction forms an angle θ_D to the polarization axis, the detected intensity is proportional to $\sin^2\theta_D$. Thus, when detecting in a small solid angle θ_C around $\theta_D = \{0, \pi\}$, the signal from the bosons is maximally suppressed. Following Brown *et al.* [17], the emission pattern for the bosonic species $\mathcal{S}^{(b)}$ is given by

$$\mathcal{S}^{(b)} = \frac{2}{3}[1 - P_2(\cos\theta_D)g(\theta_C)]\frac{1}{(\Gamma/2)^2 + (\omega - \omega_0)^2}. \quad (1)$$

TABLE I. Isotope shifts relative to ^{114}Cd, given in megahertz. Values from this paper are given with their statistical error bar in brackets, and do not include the 3.3 MHz systematic uncertainty discussed later. For fermionic isotopes, the quantum number of the excited state is given in brackets. For completeness, we include our results from Ref. [6] and add the isotope shifts of the fermionic spectral components in bold.

| | $^1P_1 \leftarrow {}^1S_0$ (229 nm) | | $^3P_1 \leftarrow {}^1S_0$ (326 nm) | |
Isotope	This paper	Literature[a]	This paper	Literature
116	−316.1(5)	−299(4)	−326.9(2)	−321.5(1.0)[b]
114	0.0(5)	0(4)	0.0(5)	0.0
113(1/2)	**147.8(4)**	148(4)	**4681.1(4)**	4653(19)[e]
				4533(23)[c]
112	407.5(7)	392(5)	426.3(3)	429.9(1.0)[b]
113(3/2)	**443.4(7)**	427(5)	**−1785.2(3)**	−1811(17)[c]
111(1/2)	**616.5(5)**	592(6)	**4982.2(9)**	4947(24)[c]
110	865.0(3)	826(6)	909.3(6)	914.7(1.0)[b]
111(3/2)	**899.2(4)**	875(6)	**−1205.3(4)**	−1217(19)[c]
108	1336.5(9)	1259(9)	1399.4(7)	1402.4(1.0)[b]
106	1818.1(1.4)	1748(11)	1911.2(2)	1913.0(1.0)[b]
111 center of gravity (c.g.)	**805.0(3)**	781(4)	**857.2(4)**	862(12)[d]
113 c.g.	**344.9(5)**	334(4)	**370.2(2)**	374(11)[d]

[a]Beam measurement, Tinsley *et al.* [22].
[b]MOT edge measurement, Ohayon *et al.* [6].
[c]Beam measurement, Kelly and Tomchuk [23].
[d]Hollow cathode discharge, relative to ^{106,108}Cd, Kloch *et al.* [24].
[e]Hanes [25].

Here, Γ is the spontaneous decay rate of the excited state, ω is the angular frequency of the laser, ω_0 is the transition angular frequency, $P_2(\cos\theta_D) = \frac{1}{2}(3\cos^2\theta_D - 1)$ is the second Legendre polynomial, and the factor $g(\theta_C) = \cos(\theta_C)\cos^2(\theta_C/2)$ accounts for the finite solid angle (half-angle θ_C) of the collection optics. In our measurements $\theta_C \approx 0.11$.

The presence of hyperfine structure in the excited states of the fermionic isotopes (which both have $I = 1/2$) has two effects. First, it changes the fluorescence emission pattern in comparison to the bosons. Upon excitation with linearly polarized light, the $F' = 1/2$ excited magnetic sublevels emit circular and linear light, which, in sum, is emitted isotropically, whereas the $F' = 3/2$ sublevels show anisotropic emission. Second, the hyperfine interval in the excited state is about 3Γ, leading to significant interference between scattering paths. This alters the observed line shape in fluorescence and can be seen as the time-averaged analog of quantum beats. To model the line shape, we again follow Brown *et al.* [17]. The fluorescence spectrum for the fermions $\mathcal{S}^{(f)}$ is given by

$$\mathcal{S}^{(f)} = \mathcal{A} + (\mathcal{B} + \mathcal{C})P_2(\cos\theta_D)g(\theta_C), \quad (2)$$

$$\mathcal{A} = \frac{1}{(\Gamma/2)^2 + \Delta_{1/2}^2} + \frac{2}{(\Gamma/2)^2 + \Delta_{3/2}^2}, \quad (3)$$

$$\mathcal{B} = -\frac{1}{(\Gamma/2)^2 + \Delta_{3/2}^2}, \quad (4)$$

$$\mathcal{C} = -\left(\frac{1}{(\Gamma/2)^2 + \Delta_{1/2}\Delta_{3/2} + i\frac{\Gamma}{2}(\Delta_{1/2} - \Delta_{3/2})} + \text{c.c.}\right), \quad (5)$$

where $\Delta_{F'} = \omega - \omega_{F'}$. Here $\omega_{F'}$ denotes the transition angular frequency to the excited-state hyperfine component F', and c.c. is the complex conjugate. The first term of Eq. (5), $\mathcal{A}$, is the emission averaged over the total solid angle, represented by a sum of Lorentzians. The second term, $\mathcal{B}$, represents the anisotropy of emission from the $F' = 3/2$ excited state. The last term, $\mathcal{C}$, accounts for the interference between decay paths. These last two terms reduce to zero by setting $\theta_D = \theta_{\text{magic}} = \arccos(\frac{1}{\sqrt{3}})$, the so-called "magic angle". To illustrate this effect, we take spectra at seven different polarization angles θ_D and compare the two models $\mathcal{S}^{(f)}$ and $\mathcal{S}^{(b)}$ to fit the observed line shapes. Figure 4(a) shows a spectrum for $\theta_D = 0$ using an enriched target (^{113}Cd). Including the interference term, i.e., using $\mathcal{S}^{(f)}$, reduces the fit residual RMS by a factor of 2. This is further substantiated by the data presented in Fig. 4(b), which shows the parameters Γ and Δ_{HF} as a function of θ_D, fitted using either a pure Lorentzian model ($\mathcal{S}^{(b)}$, red data points), or Eq. (5) ($\mathcal{S}^{(f)}$, blue data points). When a sum of two Lorentzians is used to model the line shape, the linewidth and the measured hyperfine interval vary with the polarization angle. However, when Eq. (5) is used, the polarization dependence disappears. The absolute position of the individual hyperfine components shifts by up to 20 MHz, whereas the center of gravity shifts only by about 8 MHz. We fit $e_1 + e_2 P_2(\cos\theta_D)$ to each of the data sets in Fig. 4(b). For the case of determining the hyperfine interval we get $e_2 = 25.4(3.2)$ MHz, which corresponds to a variation of 29(5) MHz, a relative variation of about 10%. For the case of the linewidth the fit yields $e_2 = 13.4(3.3)$ MHz. For the 326-nm line, the maximum expected deviation $s_{\text{Lor}}(\Delta_{\text{HF}}) \approx 0.7$ Hz. Measurements of the $^3P_1 \leftarrow {}^1S_0$ transition are, thus, not sensitive to quantum interference on a level relevant to our paper. The absolute frequencies are in this case independent of
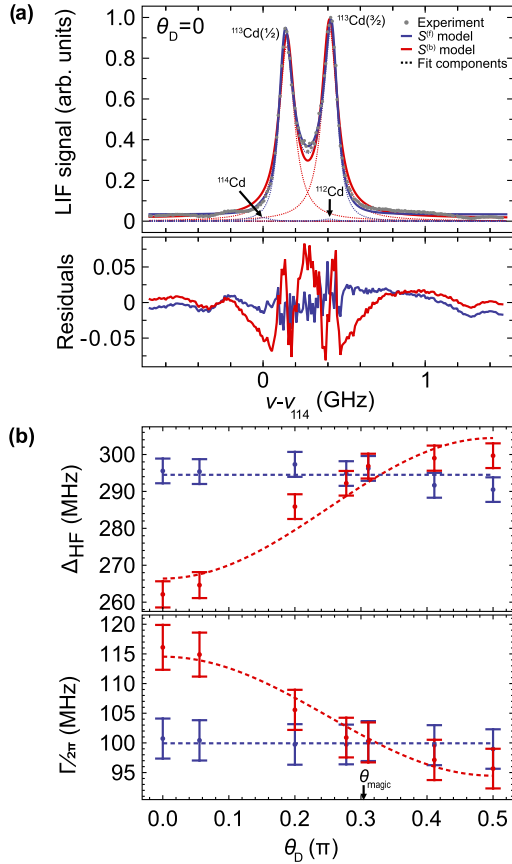
FIG. 4. Isolated hyperfine structure of the ^{113}Cd isotope, measured using an enriched target at 229 nm, plotted including the systematic error of 3.3 MHz. The quantum interference model ($\mathcal{S}^{(f)}$, blue) is compared to a sum of two Lorentzian line-shapes ($\mathcal{S}^{(b)}$, red). (a) The fit residuals reduce significantly by including quantum interference. (b) Measured hyperfine intervals Δ_{HF} and homogeneous linewidth $\Gamma/(2\pi)$ as a function of the polarization angle for the two line-shape models. Blue curves are our final result. The red dashed curve is a fit to the data.

θ_D, and we choose $\theta_D = \pi/2$ to maximize the detected boson fluorescence.

2. Isotope-shift measurement

For the measurements of the $^1P_1 \leftarrow {}^1S_0$ transition, we record a spectrum of a ^{110}Cd-enriched sample and determine the absolute transition frequency before and after each spectrum with the mixed target (see Fig. 2). The fitted ^{110}Cd line centers of all five measurements agree within the standard errors of the fits and are, thus, averaged with a standard error of 0.4 MHz. We then alternate between recording spectra of ^{110}Cd- and ^{112}Cd-enriched samples. Doing so allows us to precisely measure the IS(^{110,112}Cd) as 457.5(7) MHz (statistical uncertainty) and to reduce the number of free parameters in the fit to the spectrum of Cd with natural abundance. The number of parameters is further reduced by setting θ_D to the angle that was used in the experiment. This fixes the relative hyperfine peak amplitudes for each fermionic isotope via Eq. (5). We then fit a model that comprises a sum of eight terms, i.e., six Lorentzians ($\mathcal{S}^{(b)}$) for the bosons and two quantum interference line-shapes ($\mathcal{S}^{(f)}$) for the fermions. This model

fits the data well as demonstrated by the small fit residuals shown in Fig. 2, which are dominated by shot-to-shot fluctuations. When averaged, the fit residuals have a peak-to-peak amplitude of about 1.7%. The relative heights of the peaks are not fixed to the corresponding relative abundance in a natural sample since we expect a gradual decay of the atomic beam brightness of up to 10% over the course of a measurement. The deviation of the fitted relative abundance is consistent with this assumption.

B. Systematic uncertainty

Our measurements have a typical statistical uncertainty of $\leqslant 1$ MHz, which means we can reliably determine the line center of features in the $^1P_1 \leftarrow {}^1S_0$ transition to $\Gamma/100$. However, the wave meter we use as a frequency reference is not necessarily linear over a range of several gigahertz. We anticipate that this will be the limiting factor in the accuracy when determining relative frequencies. The hyperfine intervals of the $^3P_1$ state are known with high accuracy and already provide a good indication (see Table III). Furthermore, the ratio of the nuclear magnetic moments of Cd determines the ratio of the hyperfine intervals for different isotopes and is known with high accuracy. We perform two additional tests to estimate this uncertainty. First, we measure the hyperfine structure of ^{63,65}Cu near 327.5 and 324.8 nm, which span a frequency range of up to 12.6 GHz and are known with a precision of 10 kHz. Second, we compare the linearity of our wave meter to an ultrastable cavity. The systematic uncertainty in determining relative frequencies is estimated conservatively to be 3.3 MHz. This uncertainty is independent of the frequency span and assumed to be identical for all measurements.

1. $^3P_1 \leftarrow {}^1S_0$ nuclear magnetic moment ratios

The measured hyperfine splittings at 326 nm are given in Table III. We find good agreement with precise literature values. Furthermore, the ratio of the nuclear magnetic moments g(^{113}Cd)/g(^{111}Cd) has been determined with high accuracy to 1.0460842(2) [18]. In the approximation that hyperfine anomaly is negligible, we can assume that g(^{113}Cd)/g(^{111}Cd) = Δ_{HF}(^{113}Cd)/Δ_{HF}(^{111}Cd). For the $^1P_1 \leftarrow {}^1S_0$ transition we use this ratio as a fixed parameter. In our measurements of the $^3P_1 \leftarrow {}^1S_0$ transition, we find a ratio of 1.045 06(18) (statistical), which indicates an upper bound for the hyperfine anomaly of 4.3 MHz.

2. Hyperfine structure of copper

The D_1 (327.5-nm) and D_2 (324.8-nm) lines of Cu I lie about 1.3 nm on either side of the Cd 326-nm transition. The hyperfine splitting of the ground state is known with an accuracy of 10 kHz and has been determined to 12,568.81(1) MHz for ^{65}Cu and to 11,733.83(1) MHz for ^{63}Cu [19]. For this, we only replace the Cd ablation target in our buffer gas source with a Cu one and leave the remaining setup identical. We measure the ground-state hyperfine splitting by the method of combination differences using transition pairs involving a common excited state with total angular momentum F'. Spectra of the D_1 and D_2 lines are shown in Fig. 5(a). The difference between the extracted ground-state splitting with the
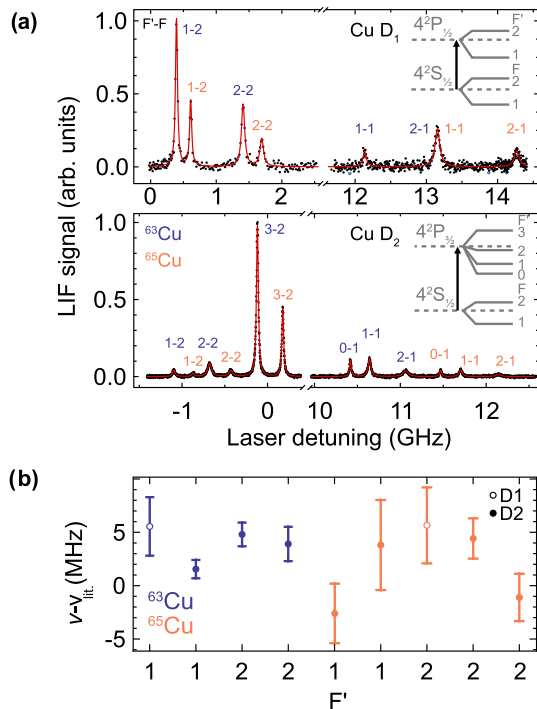
FIG. 5. Copper spectra of the D_1 and D_2 lines near 326 nm to benchmark the linearity of our wave meter. (a) Laser-induced fluorescence spectra of hyperfine transitions. Experimental data points in black and a Lorentzian fit (red curve). (b) Comparison of the measured hyperfine intervals measured via a common excited state F' to kilohertz-accuracy microwave data from Ting and Lew [19].

precisely known values are shown organized by the isotope and F' in Fig. 5(b). The mean deviation of these frequency differences is 3.1 ± 2.0 MHz for ^{63}Cu and 1.8 ± 3.7 MHz for ^{65}Cu. The weighted mean and standard error of the mean of all measurements indicates a systematic error of 3.1(1.9) MHz.

3. Stable Fabry-Pérot cavity

To measure the linearity of our wave meter with better statistics than in the previous subsections, we use a stable cavity in combination with an electro-optic modulator (EOM) that phase-modulates the laser to generate radio-frequency (RF) sidebands spaced by precisely 22.051 MHz. The cavity is a near-confocal pressure and temperature-stabilized Fabry-Pérot cavity with a Zerodur spacer, a free spectral range (FSR) of 150 MHz and a drift rate of 7.5 Hz per FSR per kelvin [20]. The high-reflectivity coating of the cavity mirrors drops sharply above 740 nm and we, therefore, tune the Ti:sa to 740 nm. Scanning the laser while monitoring the cavity transmission on a photodiode as shown in Fig. 6(a), produces a comb of resonance peaks with a known frequency spacing. By fitting the transmission peaks on the frequency axis obtained with the wave meter, the short-term (minutes) and long-term (hours) linearity of the wave meter can be determined. Figure 6(b) shows that the wave meter is close to linear for short-term scans over a single FSR and long-term scans when scanning slowly over a frequency range of about 14 GHz. Fitting to the cavity peaks gives a standard deviation of 1.0 MHz from the FSR for long-term scans [see
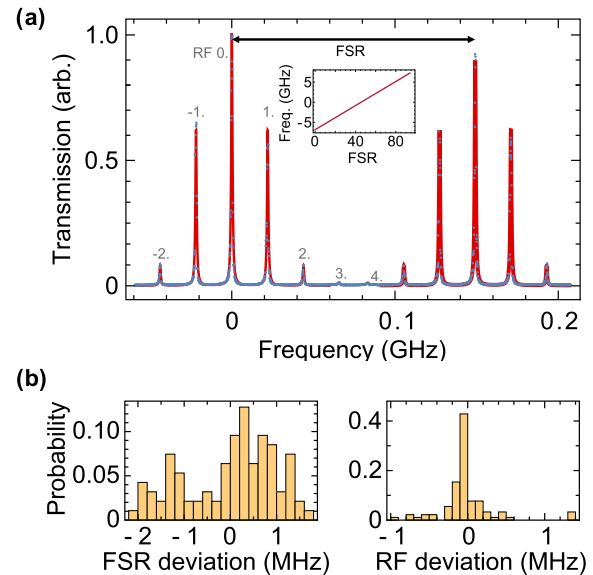

FIG. 6. Comparison of wave meter linearity to a stable Fabry-Pérot cavity. (a) Transmission through the cavity (free spectral range of about 150 MHz) at 740 nm as a function of the laser frequency. An electro-optic modulator phase modulates the laser with a fixed RF frequency. The inset compares the frequency as read by the wave meter to the number of FSR peaks. (b) The probability distribution of the residuals of a linear fit to the data has a standard deviation of 1.0 MHz. The observed spacing of the RF sidebands as measured by the wave meter has a standard deviation of 0.34 MHz.

the inset in Fig. 6(a)] and 0.34 MHz from the RF sidebands for short-term scans, which is close to the wave meter resolution of 0.4 MHz. We repeat this measurement with the ring dye laser at 652 nm. From several measurements on different days using both spectroscopy lasers, we determine a conservative upper limit for the systematic uncertainty in the determination of the relative frequencies at 229 and 326 nm of 3.3 MHz.

4. Absolute accuracy

We use a temperature-stabilized HeNe laser at 633 nm whose absolute frequency is calibrated to 5 MHz as a reference for the wave meter. Recently, we also measured the ISs of Yb to benchmark the absolute calibration and linearity of our wave meter near 399 nm [21]. The known absolute frequencies in Yb were reproduced with an accuracy of 6 MHz and the relative ISs were measured with a standard deviation of 1.3 MHz. For the 229-nm measurements presented here, we couple the frequency-doubled light of the Ti:sa (458 nm) into the wave meter to avoid the effect of intermittent multimode frequency content at the fundamental wavelength. For the 326-nm light we record the fundamental wavelength of the dye laser since fiber transmission at 326 nm is limited and influenced over time by photodegradation. We determine the absolute frequency of ^{114}Cd from a weighted average of all measurements performed. The absolute frequency for 229 nm was repeatedly found with less than 1-MHz standard deviation. For 326 nm it was reproducible over a period of nine weeks with a maximum spread of 12 MHz and a standard deviation of 5 MHz. The manufacturer specifies the absolute accuracy in the fundamental light to be 10 MHz, which we
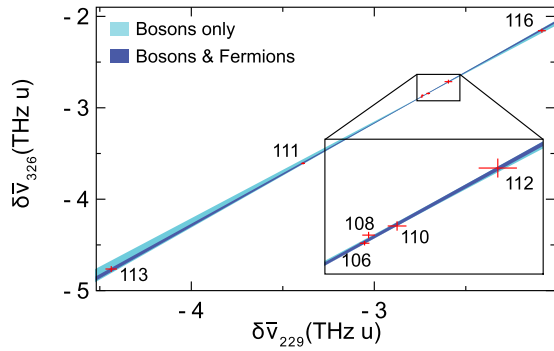
FIG. 7. King-plot analysis of the ISs of 229 and 326 nm relative to ^{114}Cd. The error bars include the systematic uncertainty in determining relative frequencies of 3.3 MHz. The shaded areas show the 68% confidence intervals for a linear fit to the bosons only (light blue). The fit including the fermions is shown in dark blue. The ISs of the fermions (center of gravity) are consistent with the extrapolated linear fit to the bosons. The inset shows a zoom in.

take as an upper bound for the uncertainty in determining absolute frequencies.

C. Results

Table I summarizes our measured ISs relative to the ^{114}Cd line and compares them to literature values. The uncertainty given is the standard error of the mean of several measurements. The values for the ISs are consistent with a recent measurement using a magneto-optical trap of Cd [6]. For the $^1P_1 \leftarrow {}^1S_0$ transition, our results are more precise than a recent measurement [22], and we observe a large discrepancy that increases linearly with the frequency. Our results for the $^3P_1 \leftarrow {}^1S_0$ transition agree well with other literature (see the overview in Ref. [26]) and are significantly more precise and accurate especially for the fermions.

1. King plot

An accurate set of ISs on two transitions can be analyzed in a King plot. Figure 7 shows such a plot using the modified IS $\delta \bar{\nu}_i^{A,A'} = \delta \nu_i^{A,A'} \mu^{A,A'}$, where $\mu^{A,A'} = 1/M_A - 1/M_{A'}$ is the nuclear mass-shift term. The linear fit has the form

$$\delta \bar{\nu}_i^{A,A'} = F_{ij} \delta \bar{\nu}_j^{A,A'} + K_{ij},$$

where F and K are the FS and MS coefficients, respectively, $F_{ij} = F_i/F_j$ is the slope and $K_{ij} = K_i - F_{ij} K_j$ is the y-axis intercept. The fit results in $F_{ij} = 1.10(3)$ and $K_{ij} = 0.13(10)$ THz u, if only the bosons are considered. Including the fermions reduces the fitting uncertainty by a factor of ≈ 3 to

$$F_{ij} = 1.117(12) \quad \text{and} \quad K_{ij} = 0.18(3) \text{ THz u}.$$

The fact that including the fermions reduces the uncertainty of the fit shows that potential shifts due to the second-order hyperfine interaction are negligible on the megahertz level. These results can be compared to CI-MBPT calculations (from preprint [27]), which yield $F_{ij} = 1.133(80)$ and $K_{ij} = 0.25(49)$ THz u. These results are consistent with ours, but our uncertainty is much lower, setting stringent benchmarks to improve the calculation. We note that the uncertainty of the

TABLE II. Nuclear charge radius difference $(\delta r^2)^{A,114}$ in fm^2 extracted from Table I with F_i and K_i from Ref. [6].

Isotope	This paper	Ref. [13]	Ref. [28]	Ref. [29]
111	−0.296(5)	−0.269(15)	−0.289(4)[a]	−0.285(4)
113	−0.118(2)	−0.101(10)	−0.116(4)[a]	−0.113(2)

[a]Our estimate is based on the reported Barret radii.

calculated field shift ratio F_{ij} is probably much smaller than our estimate based on uncorrelated error propagation as the uncertainty in the individual field shift factors is very likely to be correlated.

2. Nuclear charge radii

Our ISs for the fermions, measured using a narrow line where nearby peaks do not overlap and quantum interference is negligible, combined with the calculated negligible off-diagonal hyperfine shifts for this line [13], enable a reliable extraction for the rms charge radius difference $(\delta r^2)^{A,114}$ from the center of gravity ISs given in Table I, provided that the atomic parameters for this line are known. Here we use $F_{326} = -4354(62)$ MHz fm^{-2} and $K_{326} = 1673(43)$ GHz u obtained by projecting accurate calculations in Cd$^+$ using a King plot containing only bosons [6]. $(\delta r^2)^{A,114}$ are given in Table II. They compare reasonably well to within two combined standard deviations with those obtained through muonic x-ray measurement [28], a calibrated King plot combining muonic x rays and ISs in Cd$^+$ [11,29], and a determination based on direct calculation of F_{326} and K_{326} [13]. The slight deviation from Ref. [13] is ascribed to the fact that the calculation only reports numerical uncertainties. The slight deviation from determinations using muonic atoms is most likely due to their dependency on extrapolations of unknown higher-moment corrections from electron scattering, which has not been performed for most Cd isotopes.

3. Hyperfine intervals

Table III compares our measured hyperfine intervals for the $^1P_1$ and $^3P_1$ states with literature. For the $^1P_1$ state, we show that the spectral overlap caused a significant systematic error in previous experiments. For the $^3P_1$ state, we find that our values agree well with precise double-resonance measurements [30–32]. Recent atomic structure calculations [13,33] agree to some extent and can be benchmarked with our results.

TABLE III. Comparison of experimentally determined values for the hyperfine splitting $\Delta_{\text{HF}}(^{111}\text{Cd}, {}^{113}\text{Cd})$ in megahertz with literature values.

	229 nm		326 nm	
	^{111}Cd	^{113}Cd	^{111}Cd	^{113}Cd
This paper	282.7(3.3)	295.6(3.4)	6187.5(3.3)	6466.3(3.4)
[22,32]	285(7)	251(5)	6185.72(2)	6470.79(2)
[26]	–	–	–	6444(18)
[23]	–	–	6164(31)	6344(28)
[25]	–	–	6183(30)	6465(21)

TABLE IV. Comparison of the experimentally determined lifetime τ of the $^1P_1$ state in Cd with literature. Various indirect methods have been used for this task for nearly a century. To date, no direct measurement via the natural linewidth of the $^1P_1 \leftarrow {}^1S_0$ transition has been reported.

τ (ns)	Year [Ref.]	Method
2.00(8)	1926 [34]	Magnetorotation[a]
1.99(10)	1931 [35]	Line absorption[a]
0.38	1943 [36]	Magnetic depolarization[a]
2.10	1944 [37]	Alternating voltage[b]
1.70(9)	1950 [38]	Selective reflection
1.66(5)	1964 [39]	Hanle effect
1.11	1965 [40]	Magnetic depolarization[a]
1.66(5)	1969 [41]	Hanle effect
2.1(3)	1970 [42]	Phase shift
1.65(8)	1970 [43]	Hanle effect
1.90(15)	1973 [44]	Beam foil
1.75(20)	2004 [45]	Time-resolved fluorescence
1.60(5)	This paper	Line shape[c]

[a]This method is today known as zero-field level crossing, also known as the Hanle effect.
[b]Later referenced as the phase shift.
[c]From $\tau = \Gamma^{-1}$ with $\Gamma/(2\pi) = 99.7(3.3)$ MHz.

This also allows us to benchmark the systematic uncertainty in the linearity of our wave meter as shown in Sec. III B.

4. Radiative lifetime

The radiative lifetime of the $^1P_1$ state has been studied for almost a century. It has since been experimentally determined many times using various methods, such as the Hanle-effect or time-resolved fluorescence (see Table IV) [46]. Indirect methods used in the past to measure the lifetime of the $^1P_0$ state are more susceptible to systematic errors than a direct measurement of the line shape. Reported lifetimes range from 1.11 to 2.3 ns with an outlier at 0.38 ns. However, the authors themselves question this measurement. Nowadays, the values given by Lurio and Novick [39] and Ref. [47] [$\Gamma/(2\pi) = 95.9 \pm 2.9$ MHz] and Xu *et al.* [45] [$\Gamma/(2\pi) = 91 \pm 10$ MHz] are most commonly used in the literature.

To our knowledge, the lifetime has never been measured by fitting to a resonance line shape. Figure 4(a) shows the spectrum of an enriched ^{113}Cd ablation target. Using an enriched sample allows us to benchmark the model presented in Eq. (5), and extract the linewidth and the hyperfine interval from the fitted line shape. In addition, we determine the line shape and linewidth of the bosons by using an enriched target of ^{112}Cd (not shown), where we use Eq. (1) to fit the data. To improve the fit, we include the residual isotopes ($<2\%$), present in the enriched targets in the fit. Doppler broadening is minimized by selecting atoms with a low forward velocity between 100 and 150 ms^{-1} from the time-of-flight profile of the atomic beam. When atoms with a high forward velocity of >300 ms^{-1} are selected, the fitted linewidth remains unaffected. Fitting a Voigt profile for ^{112}Cd does improve the fit residuals and results in a value for the Lorentzian contribution consistent with a regular Lorentzian model. In total, we record eight spectra of ^{112}Cd and 11 spectra of ^{113}Cd, including the seven measurements presented

in Fig. 4. The spectral linewidths as extracted from the fits agree within the standard errors and are averaged to $\Gamma/(2\pi) = 99.7 \pm 0.6_\text{stat} \pm 3.3_\text{sys}$ MHz, which corresponds to $\tau(^1P_1) = 1.60(5)$ ns. The systematic error is discussed in Sec. III B. The Lorentzian linewidth of the spectrum of an enriched ^{110}Cd target is consistent within the 1-MHz statistical error when applying a large magnetic field ($B = 40$ G or 4 mT) parallel to the laser polarization. Zeeman broadening induced by the uncancelled magnetic field in the detection region can, thus, be neglected.

Experimentally obtained values for the lifetime of the $^3P_1$ state have been reported, at least, eight times with a weighted mean and standard error on the mean of 2.30(10) μs, corresponding to a linewidth of 69.1(27) kHz [37,48–54]. More recent literature refers to the value of Byron, Jr., *et al.* [48] which is 2.39(4) μs, corresponding to 66.6(11) kHz. Doppler broadening in our setup is two orders of magnitude larger than the natural linewidth, and we can, thus, not determine the lifetime by measuring the linewidth of the transition.

5. Absolute frequencies

The fitted line centers of spectra taken over a period of a few weeks agree with the uncertainties of the fits. Using a calibrated wave meter allows us to determine the absolute transition frequencies of the ^{114}Cd isotope for the two transitions:

$$^{114}\text{Cd}(^1P_1 \leftarrow {}^1S_0): 1,309,864,341(20)\,\text{MHz},$$

$$^{114}\text{Cd}(^3P_1 \leftarrow {}^1S_0): \quad 919,046,234(21)\,\text{MHz}.$$

The absolute frequency of the $^1P_1 \leftarrow {}^1S_0$ transition is consistent with a recent measurement (1,309,864,506(262) THz [22]) and 13 times more precise. The value given in Ref. [55] [1,309,864,580(86) THz] disagrees by about three standard deviations. The same reference [55] also lists the absolute frequency for the $^3P_1 \leftarrow {}^1S_0$ transition to 919,046,357(42) THz, which is also higher by about three times the stated standard deviation.

IV. SUMMARY

We measured the isotope shift in Cd-I for the $^1P_1 \leftarrow {}^1S_0$ and $^3P_1 \leftarrow {}^1S_0$ transitions with a statistical uncertainty of typically <1 MHz by fitting to the laser-induced fluorescence spectra from a pulsed cryogenic buffer gas-cooled atomic beam. Measurements of the $^1P_1 \leftarrow {}^1S_0$ transition are complicated by significant overlap of the spectral lines. We resolve this issue by using enriched Cd ablation targets and by suppressing the emission from the bosonic isotopes towards the direction of the detector. We determined the hyperfine intervals in the $^1P_1$ state of the fermionic isotopes and showed that quantum interference effects affect the spectral line shape. The accuracy of our wave meter is calibrated against well-known hyperfine intervals in Cd and Cu and by using a stable reference cavity in combination with an EOM. We find an upper bound of 3.3 MHz for the systematic uncertainty in measuring relative shifts. The lifetime of the $^1P_1$ state is determined spectroscopically to be 1.60(5) ns, and the absolute transition frequencies were determined with unprecedented accuracy. Our results differ significantly from recent mea-

surements, demonstrating the importance of understanding the spectral line shape and measuring the linearity of the wave meter. A King plot comprising both transitions was presented. All naturally occurring Cd isotopes follow a linear relation and the fitted slope and intercept are consistent with recent atomic structure calculations. The second-order hyperfine interaction in the fermions is negligible at the megahertz level. Combining our new measurements with recent calculations of the isotope-shift parameters allowed us to extract the fermionic isotopes' precise nuclear charge radius differences. The measurements presented here resolve significant discrepancies in the recent literature and benchmark new atomic structure calculations; a first important step towards using King plots of Cd to search for new physics beyond the standard model. A large number of naturally occurring isotopes, the presence of narrow optical transitions, and the expected small standard model background make Cd an ideal candidate for such searches.

[1] W. H. King, Comments on the article "peculiarities of the isotope shift in the samarium spectrum", J. Opt. Soc. Am. **53**, 638 (1963).

[2] C. Delaunay, C. Frugiuele, E. Fuchs, and Y. Soreq, Probing new spin-independent interactions through precision spectroscopy in atoms with few electrons, Phys. Rev. D **96**, 115002 (2017).

[3] C. Frugiuele, E. Fuchs, G. Perez, and M. Schlaffer, Constraining new physics models with isotope shift spectroscopy, Phys. Rev. D **96**, 015011 (2017).

[4] J. C. Berengut, D. Budker, C. Delaunay, V. V. Flambaum, C. Frugiuele, E. Fuchs, C. Grojean, R. Harnik, R. Ozeri, G. Perez, and Y. Soreq, Probing New Long-Range Interactions by Isotope Shift Spectroscopy, Phys. Rev. Lett. **120**, 091801 (2018).

[5] K. Ono, Y. Saito, T. Ishiyama, T. Higomoto, T. Takano, Y. Takasu, Y. Yamamoto, M. Tanaka, and Y. Takahashi, Observation of Nonlinearity of Generalized King Plot in the Search for New Boson, Phys. Rev. X **12**, 021033 (2022).

[6] B. Ohayon, S. Hofsäss, E. Padilla, S. Wright, G. Meijer, S. Truppe, K. Gibble, and B. K. Sahoo, Isotope shifts in cadmium as a sensitive probe for physics beyond the standard model, New J. Phys. **24**, 123040 (2022).

[7] S. O. Allehabi, V. A. Dzuba, V. V. Flambaum, and A. V. Afanasjev, Nuclear deformation as a source of the nonlinearity of the King plot in the Yb^+ ion, Phys. Rev. A **103**, L030801 (2021).

[8] J. Hur, D. P. A. Craik, I. Counts, E. Knyazev, L. Caldwell, C. Leung, S. Pandey, J. C. Berengut, A. Geddes, W. Nazarewicz, P.-G. Reinhard, A. Kawasaki, H. Jeon, W. Jhe, and V. Vuletić, Evidence of Two-Source King Plot Nonlinearity in Spectroscopic Search for New Boson, Phys. Rev. Lett. **128**, 163201 (2022).

[9] D. Schussheim and K. Gibble, Laser system to laser-cool and trap cadmium: towards a cadmium optical lattice clock, in *Frontiers in Optics/Laser Science* (OSA, Washington, DC, 2018).

[10] A. Yamaguchi, M. S. Safronova, K. Gibble, and H. Katori, Narrow-line Cooling and Determination of the Magic Wavelength of Cd, Phys. Rev. Lett. **123**, 113201 (2019).

[11] M. Hammen, W. Nörtershäuser, D. L. Balabanski, M. L. Bissell, K. Blaum, I. Budinčević, B. Cheal, K. T. Flanagan, N. Frömmgen, G. Georgiev, C. Geppert, M. Kowalska, K. Kreim, A. Krieger, W. Nazarewicz, R. Neugart, G. Neyens,

J. Papuga, P.-G. Reinhard, M. M. Rajabali, S. Schmidt, and D. T. Yordanov, From Calcium to Cadmium: Testing the Pairing Functional Through Charge Radii Measurements of $^{100\text{-}130}$Cd, Phys. Rev. Lett. **121**, 102501 (2018).

[12] Á. Koszorús, X. F. Yang, W. G. Jiang, S. J. Novario, S. W. Bai, J. Billowes, C. L. Binnersley, M. L. Bissell, T. E. Cocolios, B. S. Cooper, R. P. de Groote, A. Ekström, K. T. Flanagan, C. Forssén, S. Franchoo, R. F. G. Ruiz, F. P. Gustafsson, G. Hagen, G. R. Jansen, A. Kanellakopoulos, M. Kortelainen, W. Nazarewicz, G. Neyens, T. Papenbrock, P.-G. Reinhard, C. M. Ricketts, B. K. Sahoo, A. R. Vernon, and S. G. Wilkins, Charge radii of exotic potassium isotopes challenge nuclear theory and the magic character of $N = 32$, Nat. Phys. **17**, 439 (2021).

[13] J. S. Schelfhout and J. J. McFerran, Multiconfiguration dirachartree-fock calculations for Hg and Cd with estimates for unknown clock-transition frequencies, Phys. Rev. A **105**, 022805 (2022).

[14] P. Campbell, I. Moore, and M. Pearson, Laser spectroscopy for nuclear structure physics, Prog. Part. Nucl. Phys. **86**, 127 (2016).

[15] S. Truppe, M. Hambach, S. M. Skoff, N. E. Bulleid, J. S. Bumby, R. J. Hendricks, E. A. Hinds, B. E. Sauer, and M. R. Tarbutt, A buffer gas beam source for short, intense and slow molecular pulses, J. Mod. Opt. **65**, 648 (2018).

[16] S. C. Wright, M. Doppelbauer, S. Hofsäss, H. C. Schewe, B. Sartakov, G. Meijer, and S. Truppe, Cryogenic buffer gas beams of AlF, CaF, MgF, YbF, Al, Ca, Yb and NO–a comparison, Mol. Phys., e2146541 (2022).

[17] R. C. Brown, S. Wu, J. V. Porto, C. J. Sansonetti, C. E. Simien, S. M. Brewer, J. N. Tan, and J. D. Gillaspy, Quantum interference and light polarization effects in unresolvable atomic lines: Application to a precise measurement of the ^{6,7}Li D_2 lines, Phys. Rev. A **87**, 032504 (2013).

[18] P. W. Spence and M. N. McDermott, Optical orientation of 6.7h^{107}Cd, Phys. Lett. A **42**, 273 (1972).

[19] Y. Ting and H. Lew, Hyperfine structure of Cu^{63} and Cu^{65}, Phys. Rev. **105**, 581 (1957).

[20] G. Bardizza, Setup of a narrow bandwidth UV/VIS laser system for high-resolution spectroscopy of cold large molecules, M.Sc. thesis, University Milano, Milano, Italy, 2005.

[21] M. Doppelbauer, S. Wright, S. Hofsäss, B. Sartakov, G. Meijer, and S. Truppe, Hyperfine-resolved optical spectroscopy of the

$A^2\Pi \leftarrow X^2\Sigma^+$ transition in MgF, J. Chem. Phys. **156**, 134301 (2022).

[22] J. N. Tinsley, S. Bandarupally, J.-P. Penttinen, S. Manzoor, S. Ranta, L. Salvi, M. Guina, and N. Poli, Watt-level blue light for precision spectroscopy, laser cooling and trapping of strontium and cadmium atoms, Opt. Express **29**, 25462 (2021).

[23] F. M. Kelly and E. Tomchuk, Isotope shift in the CdI intercombination resonance line λ 3261 Å, Proc. Phys. Soc., London **74**, 689 (1959).

[24] R. Kloch, P. E. G. Baird, M. G. Boshier, M. J. Macpherson, C. W. P. Palmer, D. N. Stacey, and V. Stacey, Isotope shifts in λ326.1 nm of CdI, Z Phys D: At.s, Mol. Clusters **6**, 315 (1987).

[25] G. R. Hanes, Hyperfine Structure and Nucleon Configuration Assignments of Cadmium, Ph.D. thesis, University of Toronto, 1955.

[26] P. Masłowski, K. Bielska, A. Cygan, J. Domysławska, D. Lisak, R. Ciuryło, A. Bielski, and R. S. Trawiński, The hyperfine and isotope structure of the Cd intercombination line - revisited, Eur. Phys. J.l D **51**, 295 (2009).

[27] J. Z. Han, C. Pan, K. Y. Zhang, X. F. Yang, S. Q. Zhang, J. C. Berengut, S. Goriely, H. Wang, Y. M. Yu, and J. Meng, Multidimensional King-plot analysis for accurate extraction of Cd nuclear charge radii: a challenge for nuclear structure theory, arXiv:2111.04464.

[28] G. Fricke and K. Heilig, 48-Cd Cadmium, in *Nuclear Charge Radii* (Springer-Verlag, Berlin, 2004), pp. 1–9.

[29] J. Z. Han, C. Pan, K. Y. Zhang, X. F. Yang, S. Q. Zhang, J. C. Berengut, S. Goriely, H. Wang, Y. M. Yu, J. Meng, J. W. Zhang, and L. J. Wang, Isotope shift factors for the $Cd^+ 5s^2 S_{1/2} \rightarrow 5p^2 P_{3/2}$ transition and determination of Cd nuclear charge radii, Phys. Rev. Res. **4**, 033049 (2022).

[30] R. F. Lacey, Investigation of the (5S5P) $^3P_1$ Level of Cadmium., Ph.D. thesis, Massachusetts Institute of Technology, 1952.

[31] R. J. Hull, H. H. Stroke, R. F. Lacey, and H. R. Hirsch, Nuclear magnetic resonance and hyperfine structure, Tech. Rep. [Research Laboratory of Electronics (RLE) at the Massachusetts Institute of Technology (MIT), 1959], hdl.handle.net/1721.1/52258.

[32] P. Thaddeus and R. Novick, Optical detection of level crossing in the (5s5p)$^3P_1$ state of Cd^{111} and Cd^{113}, Phys. Rev. **126**, 1774 (1962).

[33] B. Lu and H. Chang, Theoretical calculations on Landé g-factors and quadratic Zeeman shift coefficients of nsnp $^3P_0^o$ clock states in Mg and Cd optical lattice clocks, Chin. Phys. B **32**, 013101 (2022).

[34] W. Kuhn, Intensität von Absorptionslinien in Cadmiumdampf, Naturwissenschaften **14**, 48 (1926).

[35] M. W. Zemansky, Absorption der Cadmium-Resonanzstrahlung λ = 2288 Å und Lebensdauer des Cd 2$^1P_1$-zustandes, Z. Phys. **72**, 587 (1931).

[36] P. Soleillet and J. Ploquin, Sur une durée de vie très courte de l'atome de cadmium à l'état excité par la raie 2288 Å, Comptes Rendus Hebdomadaires Des Seances De L'Académie Des Sciences **217**, 368 (1943).

[37] H. W. Webb and H. A. Messenger, Lifetimes of resonance lines of cadmium, Phys. Rev. **66**, 77 (1944).

[38] H. L. Welsh, J. Kastner, and A. C. Lauriston, Selective reflection from mercury and cadmium vapors, Can. J. Res. **28a**, 93 (1950).

[39] A. Lurio and R. Novick, Lifetime and hfs of the (5s5p)$^1P_1$ state of cadmium, Phys. Rev. **134**, A608 (1964).

[40] M. Spitzer, Duree de vie de letat excite dans le cadmium par la raie de resonance 2288 Å, Comptes Rendus Hebdomadaires Des Seances De L'Académie Des Sciences **260**, 3907 (1965).

[41] H. Saussereau and M. Barrat, Effective sections of cadmium atom depolarization at level-5$^1P_1$ during collisions with rare gases, Comptes Rendus Hebdomadaires Des Seances De L'Académie Des Sciences Serie B **268**, 475 (1969).

[42] S. R. Baumann and W. H. Smith, Atomic transition probabilities - ultraviolet multiplets of Zn I,II and Cd I,II, J. Opt. Soc. Am. **60**, 345 (1970).

[43] R. Pepperl, Relaxation of 5$^1P_1$-state of cadmium in collisions with noble gas atoms and hydrogen molecules, Zeitschrift für Naturforschung A **25**, 927 (1970).

[44] T. Andersen and G. Sørensen, Systematic trends in atomic transition probabilities in neutral and singly ionized zinc, cadmium and mercury, J. Quant. Spectr. Radiat. Trans. **13**, 369 (1973).

[45] H. L. Xu, A. Persson, S. Svanberg, K. Blagoev, G. Malcheva, V. Pentchev, E. Biemont, J. Campos, M. Ortiz, and R. Mayo, Radiative lifetime and transition probabilities in CdI and CdII, Phys. Rev. A **70**, 042508 (2004).

[46] One of the first values was measured by Ref. [35] at the Kaiser-Wilhelm-Institut für physikalische Chemie und Elektrochemie, the original name of what currently is the Fritz Haber Institute of the Max Planck Society.

[47] Thaddeus and Novick [32] cite Lurio and Novick [39] as private communication with a slightly different value. In Table IV we use the published value.

[48] F. W. Byron, Jr., M. N. McDermott, and R. Novick, Self-broadening of optical double resonance lines in cadmium, Phys. Rev. **134**, A615 (1964).

[49] W. E. Van der Veer, D. P. Van der Blonk, and A. Donszelmann, Determination of the radiative properties of the 5s5p$^3P_1$ and the 5s6s$^3S_1$ levels in cadmium, Astron. Astrophys. **231**, 277 (1990).

[50] A. R. Schaefer, Measured lifetimes of excited states in Cd, J. Quant. Spectrosc. Radiat. Transfer **11**, 197 (1971).

[51] H. D. Koenig and A. Ellett, Direct measurement of mean lives of atomic states, Phys. Rev. **39**, 576 (1932).

[52] M. Czajkowski, R. Bobkowski, and L. Krause, $O_u^+(^3\Pi_u) \leftarrow XO_g^+(\Sigma_g^+)$ transitions in Cd$_2$ excited in crossed molecular and laser beams, Phys. Rev. A **40**, 4338 (1989).

[53] E. Ceneux and B. Wanders-Vincenz, Etude par le résonance magnétique dans des jets atomiques, d'états excités de l'atome de cadmium, Helv. Phys. Acta **33**, (1960).

[54] C. G. Matland, Natural lifetime of the cadmium 5$^3P_1$ state, Bull. Amer. Phys. Soc. **28**, 3 (1953).

[55] K. Burns and K. B. Adams, Energy levels and wavelengths of natural cadmium and of cadmium-114, J. Opt. Soc. Am. **46**, 94 (1956).

[56] https://doi.org/10.5281/zenodo.7519878.